PAPER

Check for updates

Amine functionalized quinolinium polyoxometalates as highly active heterogeneous catalysts for solvent-free CO_2 cycloaddition and Knoevenagel condensation reactions†

Kousik Routh, Rajesha Kumar Swain, Gaurav Kumar and Chullikkattil P. Pradeep ⓘD *

Introducing task-specific catalytic sites through rational design is paramount while developing a multi-functional catalyst for organic transformation reactions. In this work, we utilized rarely explored quinolinium counterions to build a new class of quinolinium-polyoxometalate (POM) hybrids and test their catalytic activities in various organic transformation reactions. We introduced a task-specific '$-NH_2$' functional group onto the quinolinium moiety to enhance basic and hydrogen bonding sites towards the catalytic reactions and developed a series of POM-hybrids $(ACMQ)_4[H_2V_{10}O_{28}]$ (hybrid **1**), $(ACMQ)_4[SiMo_{12}O_{40}]$ (hybrid **2**) and $(ACMQ)_4[SiW_{12}O_{40}]$ (hybrid **3**) (where ACMQ = 4-amino-7-chloro-1-methylquinolin-1-ium) starting from common POM precursors. These hybrids were tested as catalysts for two organic transformation reactions: the cycloaddition of CO_2 to epichlorohydrin (ECH) to form epichlorohydrin carbonate, and the Knoevenagel condensation of benzaldehyde with malononitrile to yield 2-benzylidene malononitrile. Hybrid **1**, containing the decavanadate cluster, showed the best catalytic activity among the hybrids tested toward the CO_2 cycloaddition reaction, yielding cyclic carbonates in 96% yield with a turnover number (TON) of 834 at ambient temperature and pressure in solvent-free, neat conditions. This hybrid also showed the best catalytic performance with high conversion (96%) and a high turnover of 5647 in the Knoevenagel condensation reaction of benzaldehyde with malononitrile at room temperature using an eco-friendly solvent, ethanol. A control compound, hybrid **4** $((DCMQ)_4[H_2V_{10}O_{28}])$, prepared using the decavanadate cluster and a quinolinium counterion, 4,7-dichloro-1-methylquinolin-1-ium (DCMQ) bearing a $-Cl$ moiety in place of the $-NH_2$ on ACMQ, showed negligible catalytic activity in both these reactions, emphasizing the role of '$-NH_2$' functionality of the counterions in determining the better catalytic performance of hybrid **1**. Additionally, hybrid **1** showed structural stability in up to five catalytic cycles in both reactions. The presence of multiple catalytic sites on hybrid **1**, *i.e.*, the basic oxygen surface of the clusters and the '$-NH_2$' functional group of the quinolinium counterions that can act as both basic sites as well as hydrogen bond donors to activate different substrates, is expected to play a significant role in its catalytic performance. Most importantly, in this study, the hybrid catalysts were synthesized in water at room temperature, and the catalytic reactions were conducted either under neat conditions or in ethanol, marking a significant step toward sustainability in catalyst synthesis and reactions.

School of Chemical Sciences, Indian Institute of Technology Mandi, Kamand – 175005, Himachal Pradesh, India. E-mail: pradeep@iitmandi.ac.in;
Fax: +911905267 009; Tel: +91 1905 267 045

Introduction

Several organic transformation reactions require the simultaneous activation of different reactants by a catalyst to achieve better yields. Therefore, introducing task-specific catalytic sites through rational design is paramount while developing a catalyst for organic transformation reactions. Multifunctional catalytic systems, which incorporate multiple catalytic centers such as acidic and basic sites, are often more effective than single-site catalysts.[1] The biggest challenge in developing such multicenter catalysts is assembling the different catalytic sites in a single entity. Various techniques have been employed to

assemble multifunctional catalysts, including direct co-condensation, post-grafting, and encapsulation. Bifunctional catalytic systems based on diverse materials, such as metal–organic frameworks (MOFs), polyoxometalate-organic frameworks (POMOFs), covalent organic frameworks (COFs), zeolites, amine-functionalized graphitic carbon nitrides, and ionic liquids, have been reported recently.[2–7] Sustainable synthetic procedures involving minimal or no toxic solvents are another essential aspect when designing a catalyst. Green synthetic conditions are generally preferred for catalyst synthesis and catalytic reactions. If strict sustainability criteria are to be applied, many of the catalysts mentioned above may fail, as they are typically synthesized at high temperatures or pressures using toxic organic solvents.[6,8–10] Therefore, developing sustainable procedures for catalyst synthesis and conducting catalytic reactions using eco-friendly solvents under ambient conditions is crucial.

The increasing levels of CO_2 in the atmosphere are considered a significant contributor to global warming.[11] Conversely, CO_2 has been recognized as a cheap, non-flammable, inexhaustible carbon source and a C1 building block.[12] There are several well-established strategies for converting CO_2 into valuable products, the most common being the storage of CO_2 as five-membered cyclic carbonates by reacting it with epoxides. Many cyclic carbonates are versatile and eco-friendly solvents in lithium-ion batteries, polycarbonate plastics, and various chemical syntheses.[13–15] CO_2 cycloaddition reactions typically require high temperatures and pressures due to the thermodynamic stability and kinetic inertness of CO_2, necessitating a catalyst to reduce the activation energy. Ideally, such a cycloaddition catalyst should possess both acidic and basic sites to activate the epoxide and the CO_2.[16] Meanwhile, the Knoevenagel condensation reaction is an important and useful synthetic tool in organic chemistry. The C=C bond formation is commonly achieved using the Knoevenagel condensation reaction, which involves the addition of a carbon nucleophile to a carbonyl function, followed by dehydration.[16,17] The α,β-unsaturated products obtained from the Knoevenagel condensation reaction are widely used as intermediates in producing fine chemicals, natural products, insecticides, therapeutic agents, coumarin derivatives, polymers in the cosmetic industry, and pesticides.[18–21] Knoevenagel condensation needs a base, such as primary, secondary, or tertiary amines, or any other organic or inorganic base, that can abstract a proton from the methylene compound, forming a carbanion. On the other hand, an acidic center or a primary amine can activate the carbonyl group of the second substrate, enabling the carbanion to form a bond with the carbonyl group.[6] Therefore, both the reactions mentioned above, i.e., the cycloaddition of CO_2 to epoxides and the Knoevenagel condensation reaction, may be accelerated by using bifunctional catalysts with multiple active sites to activate electrophiles and nucleophiles simultaneously.

Polyoxometalates (POMs) are discrete, soluble metal oxide clusters formed by early transition metals V, Nb, Ta, Mo, W, etc., in their highest oxidation state.[22,23] The acidity and basi-

city of POMs can vary based on the metals and the overall negative charge on the cluster.[24] POMs with Lewis acidic transition metal centers can interact with CO_2 efficiently using the acidic metal sites. Similarly, the high density of oxygen atoms on the surface of POMs can act as a potential basic site, effectively activating CO_2.[25–27] However, the POM-derived basic catalysts have scarcely been investigated because most POMs show only weak basic properties. Some theoretical studies have shown that the basic strength of POM anions increases with the negative charges on POMs. Accordingly, Mizuno et al. used lacunary POMs with high negative charge as efficient basic catalysts for the Knoevenagel condensation reaction.[28] POMs based on Group V metals exhibit a large anionic charge and are proposed as better Lewis base catalysts compared to other POM-based catalysts. For example, Tsukuda et al. reported a decaniobate cluster $((TBA)_6[Nb_{10}O_{28}]$ (TBA^+ = tetrabutylammonium cation)) which adsorbs CO_2 on the surface of the POM cluster and acts as a Lewis base catalyst in the CO_2 cycloaddition reaction.[27] Another approach to improve the overall catalytic sites of POMs is to combine them with other organic/metal–organic moieties, leading to novel POM-organic hybrid materials. Developing POM-based hybrids is also helpful in addressing some of the common issues in POMs-based catalysis, such as the difficulties in catalyst/product separation, product contamination, poor processability, etc.[29] Accordingly, there are a few reports on the POM-based organic–inorganic hybrid materials modified with organic/organometallic moieties bearing acidic or basic sites for CO_2 cycloaddition and Knoevenagel condensation reactions. In 2019, Xu and co-workers first reported a windmill-shaped V8 cluster surrounded by amine functionality as an efficient catalyst for the cycloaddition of CO_2.[30] Dong et al. reported that increased amounts of V^{4+} centers in a mixed V^{4+}/V^{5+} catalytic system lead to an increase in the surface acidity of the catalyst.[31–33] Zhou et al. have reported a hybrid structure based on 2D polyoxovanadate (POV), in which two geometrically and structurally different POVs are interconnected by a hydrated Ln^{3+} and Ln-dpdo metal–organic linker. Additionally, they demonstrated that all the catalysts exhibited good catalytic conversion in the Knoevenagel condensation reaction, attributed to the Lewis acidity of Ln^{3+} cations and the Lewis basicity of the POM cluster.[8] It is worth noting that many of the POM hybrids mentioned above were synthesized under hydrothermal conditions at high temperatures and pressures. Therefore, strategies to introduce functional moieties onto POMs to enhance their catalytic properties using milder conditions would be highly desirable.

Herein, we synthesized a set of POM-based class I hybrids[34] having a task-specific amine functional group on organic counterions (OCIs) using water and ethanol as solvents at room temperature. In this study, we utilized a rarely explored class of OCIs, specifically quinolinium counterions, in conjunction with a series of polyoxometalate (POM) clusters featuring different metal centers, to investigate the roles of various catalytic sites within the POM hybrids in determining their catalytic activities. We developed a new quinolinium-
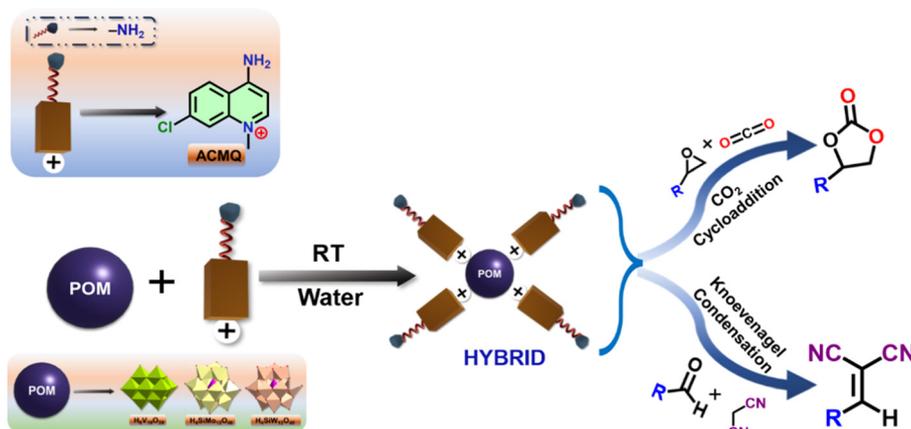
Scheme 1 Outline of the synthesis and applications of hybrids **1–3**.

based OCI, *i.e.*, ACMQ (where ACMQ = 4-amino-7-chloro-1-methylquinolin-1-ium), bearing an –NH$_2$ functional group and clubbed it with common and readily available POM clusters such as decavanadate ([V$_{10}$O$_{28}$]$^{6-}$) cluster, silicomolybdic acid ([SiMo$_{12}$O$_{40}$]$^{4-}$), and silicotungstic acid ([SiW$_{12}$O$_{40}$]$^{4-}$) in a water medium at room temperature (see Scheme 1) to generate the hybrids having the formula (ACMQ)$_4$[H$_2$V$_{10}$O$_{28}$] (hybrid **1**), (ACMQ)$_4$[SiMo$_{12}$O$_{40}$] (hybrid **2**), and (ACMQ)$_4$[SiW$_{12}$O$_{40}$] (hybrid **3**). All the hybrids were tested as catalysts for the organic transformation reactions, *i.e.*, CO$_2$ cycloaddition and Knoevenagel condensation reactions. Among all the hybrids tested, hybrid **1**, featuring the decavanadate cluster, exhibited remarkable activity towards the cycloaddition of CO$_2$ to epichlorohydrin (ECH), resulting in a cyclic carbonate yield of 96% in 12 hours with a turnover frequency (TOF) of 69.6 h^{-1} under ambient temperature and pressure in solvent-free, neat conditions. Furthermore, hybrid **1** also exhibited the best catalytic activity in the Knoevenagel condensation reaction, converting benzaldehyde to 2-benzylidine malononitrile with a yield of up to 96%, and a TOF value of 1882.36 h^{-1} at room temperature, using ethanol as the solvent.

Results and discussion

Synthesis and characterization

The hybrids (ACMQ)$_4$[H$_2$V$_{10}$O$_{28}$] (hybrid **1**), (ACMQ)$_4$[SiMo$_{12}$O$_{40}$] (hybrid **2**), and (ACMQ)$_4$[SiW$_{12}$O$_{40}$] (hybrid **3**) were synthesized by dropwise addition of a solution of ethanol–water mixture of ACMQI to an aqueous solution of the respective POM cluster, leading to the precipitation of the hybrid as a powder. The precipitated product was then filtered and washed successively with water, ethanol, and diethyl ether, followed by drying under vacuum to obtain the hybrids **1–3**. The successful synthesis of the hybrids was confirmed by FT-IR, XPS, ESI-MS, and SC-XRD analysis. The FT-IR spectra of hybrids **1–3** are shown in Fig. S17, ESI.† The characteristic peaks due to the symmetric and asymmetric stretch of the

N–H bond of the organic counterion ACMQ appeared in the range of 3500–3300 cm^{-1}. Similarly, the bands observed in the ranges 1653–1641 cm^{-1} and 1532–1453 cm^{-1} are due to the C=N and C=C bond stretch of the counterion moiety, respectively. In the case of hybrid **1**, the decavanadate cluster showed its characteristic ν_s(V–O$_t$) and ν_{as}(V–O$_b$–V) stretching vibrations in the range of 946–940 cm^{-1} and 819–738 cm^{-1}, respectively.[35] For hybrid **2**, the bands observed at 950 cm^{-1} and 895–779 cm^{-1} correspond to ν_s(Mo–O$_t$) and ν_{as}(Mo–O$_b$–Mo), respectively.[36] FT-IR of hybrid **3** showed bands in the range of 970–775 cm^{-1} due to ν_s(W–O$_t$) and ν_{as}(W–O$_b$–W) vibrations of the cluster.[36]

The NMR analysis of hybrids **1–3** was performed in DMSO-d$_6$, which confirmed the presence of both counterions and the POM cluster (see Fig. S9–S11, ESI†). The ESI-MS of hybrids **1–3** was performed in negative ion mode. The solutions for ESI-MS analyses were prepared by dissolving small quantities of hybrids in DMSO followed by diluting with acetonitrile to achieve a final concentration of approximately 10^{-6} M. ESI-MS data of hybrids **1–3** showed peaks at *m/z* 462.6774, 606.5924 and 718.3191 corresponding to [V$_{10}$O$_{26}$]$^{2-}$, H[SiMo$_{12}$O$_{40}$]$^{3-}$, and [SiW$_{12}$O$_{40}$]$^{4-}$, respectively. The peaks observed for hybrids **1–3** at *m/z* 1154.4259, 1463.3136, and 1562.7102 revealed the presence of [(ACMQ)$_8$H(V$_{10}$O$_{28}$)$_2$]$^{3-}$, [(ACMQ)$_3$NaK(SiMo$_{12}$O$_{40}$)$_2$(H$_2$O)$_6$]$^{3-}$, and [(ACMQ)K(SiW$_{12}$O$_{40}$)(H$_2$O)]$^{2-}$, respectively. Detailed mass data are provided in Fig. S13–S15 of the ESI.†

X-ray photoelectron spectroscopy (XPS) analyses of hybrids **1–3** were conducted to confirm the presence of OCIs and POM clusters in the hybrids. Carbon C 1s scans were used as an internal reference to calibrate the XPS spectra. XPS survey of hybrids **1–3** revealed the presence of carbon, nitrogen, oxygen, chlorine, and the corresponding transition metals (Mo, W, V) in the hybrid cluster; see Fig. S20, ESI.† To confirm the quinolinium counterions in hybrids **1–3**, we deconvoluted their C 1s, N 1s, and Cl 2p spectra. Deconvoluted C 1s spectra of all hybrids (hybrids **1–3**) showed peaks at 284.8, 286.2, and 291.2–290.7 eV, corresponding to C=C/C–C, C=N, and shake-up peaks, respectively. Furthermore, the N 1s scan of hybrids

1–3 showed two peaks near 399.2–396.5 eV and 400.7–398.9 eV, corresponding to C=N–C and C–NH$_2$, respectively.[36] Finally, deconvoluted Cl 2p of hybrids **1–3** showed doublets at 200.6–200.1 eV and 202.26–201.69 eV, corresponding to Cl 2p$_{3/2}$ and Cl 2p$_{1/2}$, respectively, which concluded the presence of the organic counterions in the hybrids as expected. In the case of hybrid **1**, deconvoluted V 2p XPS spectra showed peaks at around 516.79–516.59 eV, 516.37–515.83 eV, 524.30–523.81 eV, and 523.16 eV corresponding to V^{5+} 2p$_{3/2}$, V^{4+} 2p$_{3/2}$, V^{5+} 2p$_{1/2}$, and V^{4+} 2p$_{1/2}$, respectively. Further, deconvoluted Mo 3d spectra of hybrid **2** showed peaks at 232.36, 232.84, 235.09, and 235.95 eV corresponding to Mo^{5+} 3d$_{5/2}$, Mo^{6+} 3d$_{5/2}$, Mo^{5+} 3d$_{3/2}$, and Mo^{6+} 3d$_{3/2}$, respectively.[37] Finally, hybrid **3** showed deconvoluted W 4f peaks at 35.06, 35.79, 37.05, and 37.93 eV, indicating the presence of W^{5+} 4f$_{7/2}$, W^{6+} 4f$_{7/2}$, W^{5+} 4f$_{5/2}$ and W^{6+} 4f$_{5/2}$, respectively; see Fig. S19, ESI.†[38] The XPS spectral analyses, therefore, confirm the presence of organic counterions and the POM units in hybrids **1–3**, as expected.

Single-crystal X-ray diffraction analyses

Single crystals of hybrid **1** suitable for XRD analysis were grown from DMF solutions by a slow evaporation method. Hybrid **1** crystallized in the triclinic crystal system with $P\bar{1}$ space group. The asymmetric unit of hybrid **1** contains a half cluster of decavanadate [H(V$_5$O$_{14}$)]$^{2-}$ surrounded by two ACMQ counterions, one dimethyl formamide solvent molecule, and one water molecule; see Fig. 1(a). Both counterions with '–NH$_2$' functionality engage in hydrogen bonding interactions

with the POM cluster. The distances between the amine groups in the counterions and the POM cluster are summarized in Table S3 of the ESI.† These distances, for example, 2.05 Å for H2A(N2)···O8 and 1.99 Å for H4B(N4)···O5, suggest relatively strong hydrogen bonding interactions. The packing diagram (view along 'a' direction) of hybrid **1** showed a 2D layered structure; see Fig. 1(e). Furthermore, the quinoline rings of the OCIs exhibited π–π stacking interactions, resulting in a compact layered structure, as shown in Fig. 1(d). Single crystals of hybrids **2** and **3** were grown from dimethylformamide solvent through the diethyl ether diffusion method. Both these hybrids crystallized in the monoclinic $P2_1/n$ space group. The asymmetric unit of hybrids **2** and **3** contains one Keggin cluster (*i.e.*, [SiMo$_{12}$O$_{40}$]$^{4-}$ in hybrid **2** and [SiW$_{12}$O$_{40}$]$^{4-}$ in hybrid **3**) surrounded by four ACMQ counterions, and one DMF and two water molecules in hybrid **2** and six DMF molecules in hybrid **3**; see Fig. 1(b) and (c). The packing diagram and π–π stacking interactions of hybrids **2** and **3** are given in Fig. S57, ESI.†

The thermal stability of hybrids **1–3** was investigated using thermogravimetric (TGA) analysis. The samples were scanned in the 25–800 °C temperature range under a nitrogen atmosphere with a scan rate of 10 °C min^{-1}. TGA data of all hybrids revealed the elimination of water molecules at around 100 °C. Hybrid **1** was stable up to 200 °C, and in the temperature range of 200–530 °C, it lost four counterions (calc. 44.67% and obs. 43.88%). At 600 °C, all the POM clusters decomposed and formed metal oxides, following a similar trend reported for
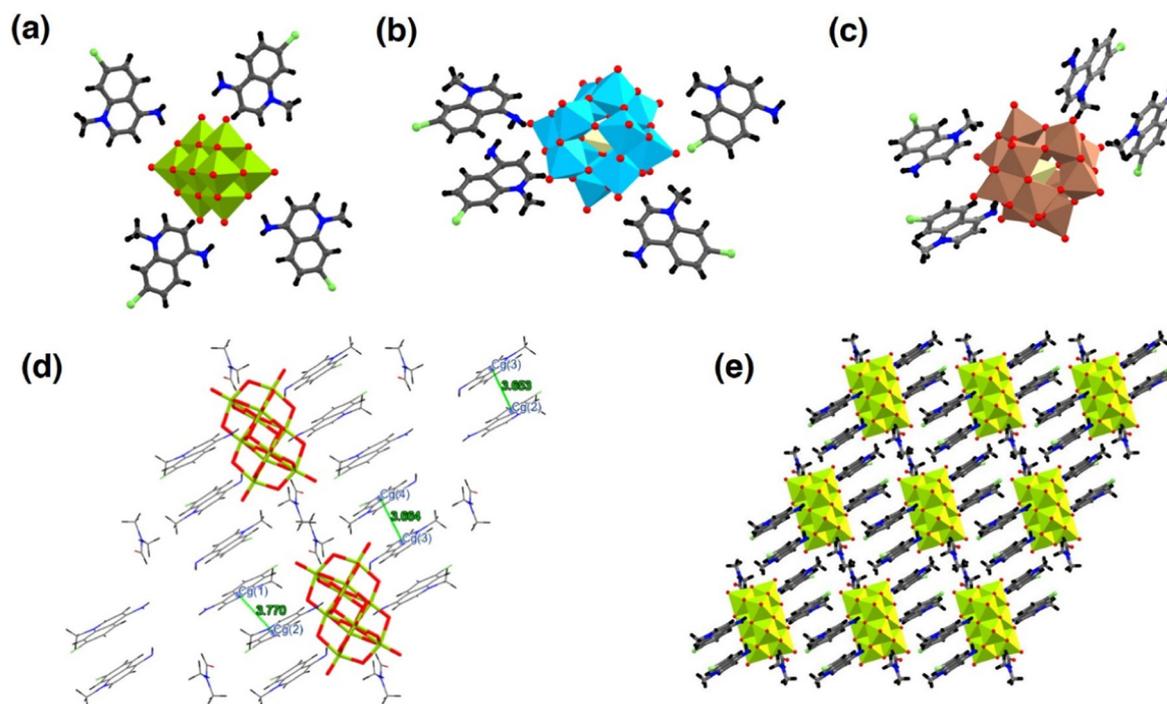

Fig. 1 (a) Crystal structure of hybrid **1**; (b) crystal structure of hybrid **2**; (c) crystal structure of hybrid **3**; (d) π–π stacking interactions in hybrid **1**; (e) packing diagram of hybrid **1** showing a view along 'a' axis. Color code: VO^{6-} green polyhedra; MoO^{6-} light blue polyhedra; WO^{6-} light brown polyhedra; carbon – light grey; oxygen – red; nitrogen – pink; chlorine – light green; hydrogen – black.

decavanadate-based POM hybrid clusters.[39] TGA data of hybrids **1–3**, presented in Fig. S21 (ESI),† showed different thermal stabilities due to the presence of different POM units.[40]

Surface area and temperature programmed desorption (TPD) analysis of hybrids 1–3

We performed the Brunauer–Emmett–Teller (BET) surface area analysis of hybrids **1–3** to measure their surface area. The BET surface areas of hybrids **1–3** were measured using N_2 gas adsorption–desorption isotherms at 77 K; see Fig. 2(a). Hybrid **1** showed the highest BET surface area of 32.436 m^2 g^{-1}, followed by hybrid **2** (14.890 m^2 g^{-1}) and hybrid **3** (3.542 m^2 g^{-1}).[41] To determine the accessible Lewis basic sites of the POM hybrids, we examined CO_2 adsorption–desorption isotherms for hybrids **1–3** at 298 K; see Fig. 2(b). These analyses revealed a maximum CO_2 uptake by hybrid **1** (8.28 mg g^{-1}), followed by hybrid **2** (3.71 mg g^{-1}) and hybrid **3** (1.67 mg g^{-1}) (see Fig. S55, ESI†), suggesting a strong interaction between CO_2 and the active basic sites of hybrid **1**. To calculate the amount of basic sites present, we performed a CO_2-TPD (Temperature Programmed Desorption) analysis on hybrids **1–3**. The CO_2-TPD analysis of hybrid **1** showed two strong peaks at 161 °C and 174 °C, indicating a medium basic strength. However, the other hybrids (hybrids **2** and **3**) did not show such peaks in the same temperature range, indicating a higher basicity for hybrid **1**; see Fig. S56, ESI.† It is worth noting that POMs based on Group V metals have a significantly larger anionic charge compared to W- or Mo-based POMs, making them potential candidates for Lewis-base catalysis.[27,42] In a previous report, it has been suggested that common Keggin clusters with a lower negative charge and

fewer basic sites are inactive for CO_2 conversion.[43] Hence, we can conclude that the basicity of the decavanadate cluster is crucial in increasing CO_2 adsorption capacity and may influence the CO_2 cycloaddition reaction. We also calculated the number of acidic sites on hybrid **1** using NH_3-TPD analysis. Our findings showed that the total number of basic sites (0.748 mmol g^{-1}) exceeds that of acidic sites (0.612 mmol g^{-1}). This observation further suggests that the enhanced basic sites in hybrid **1** may play a significant role in determining the rate of the CO_2 cycloaddition reaction and in base-mediated catalysis reactions such as the Knoevenagel condensation reaction.

Catalytic conversion of CO_2

The hybrids **1–3** bear four '–NH_2' functional groups in total on their counterions. The amino functional groups are effective hydrogen bond donors, capable of activating epoxides through hydrogen bonding interactions.[40] Furthermore, the amino groups are known to interact with CO_2 molecules.[44,45] Additionally, the basic POM cluster oxygens can also help activate the CO_2 molecules. Apart from these, some of the reduced metal centers, especially reduced vanadium centers (V^{4+}), are reported to enhance the overall surface acidity of certain vanadium-containing catalytic systems.[33] The V^{4+} centers may help to create Brønsted acidic sites by polarizing intervening small molecules.[32] The presence of these different catalytically active sites on hybrids **1–3** prompted us to test their catalytic performance toward the cycloaddition of CO_2 to epoxide (epichlorohydrin (ECH)) under mild conditions. We chose to use tetrabutylammonium bromide (TBAB) as a cocatalyst in the CO_2 cycloaddition reaction, despite its drawbacks, such as potential for halide-mediated corrosion and toxicity.[46,47] This
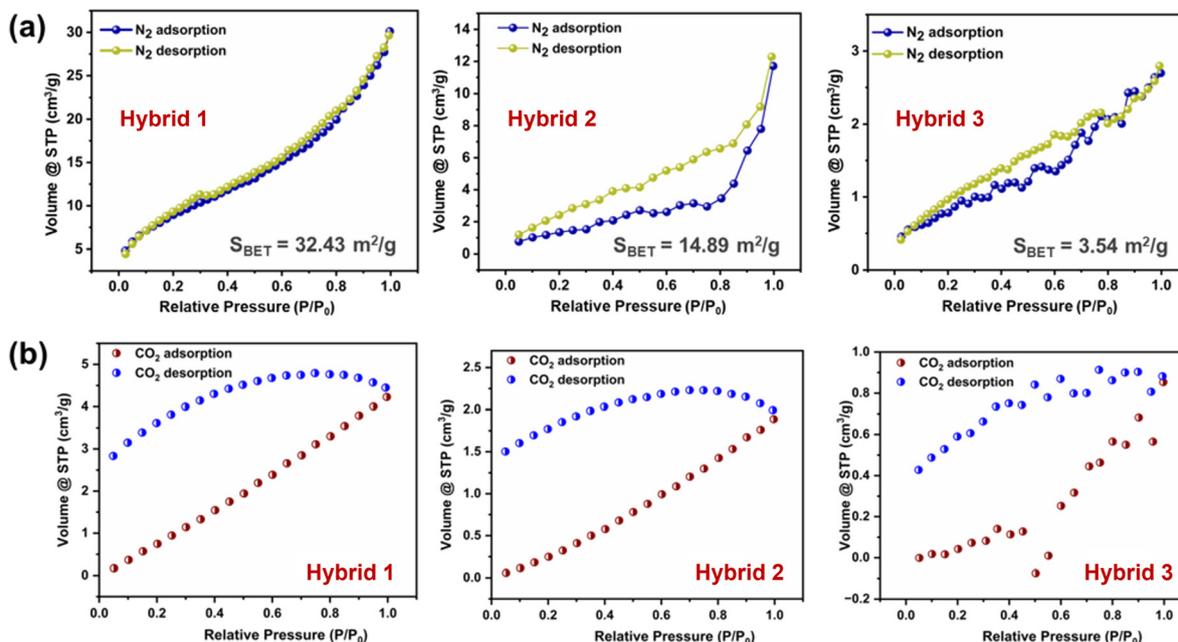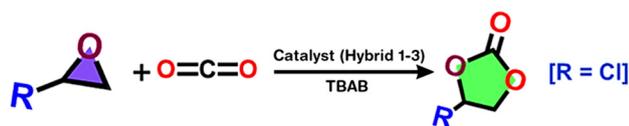

Fig. 2 (a) N_2 adsorption–desorption isotherm of hybrids **1–3** (at 77 K); (b) CO_2 adsorption–desorption isotherm of hybrids **1–3** (at 298 K).

decision is influenced by the fact that several of the reported halide-free catalysts employed in CO_2 cycloaddition reactions typically require extreme conditions, including high temperatures and pressures.[48,49] Our selection of cocatalyst is also based on the superior nucleophilicity of the Br^- ion, coupled with the advantage of milder reaction conditions that effectively facilitate the attack on the epoxide ring.[50] Therefore, we used hybrid **1** as the model catalyst, and TBAB as a co-catalyst to optimize the reaction conditions; see Scheme 2.

Initially, we optimized the reaction conditions by altering parameters such as the reaction temperature, catalyst dosage, cocatalyst amount, and reaction time. In all the reactions, the reaction products were analyzed using ^1H NMR spectroscopy. For that, the crude reaction mixture was carefully pipetted from the reaction vessel (stoppered glass vials) and centrifuged to separate the catalyst. The supernatant liquid portion was then collected and dissolved in an appropriate NMR solvent ($CDCl_3$, 650 μL) to minimize potential product loss. The product yields were calculated based on the proton count obtained from the NMR spectra. Detailed results are presented in Table 1. First, the reaction was carried out under neat conditions at three different temperatures: 30 °C, 50 °C, and 70 °C for 12 hours. The catalyst, cocatalyst, and substrate dosages were kept at 0.115 mol%, 0.62 mol%, and 10 mmol, respectively, in all the cases. At 30 °C, the conversion of ECH to its carbonate ECHC (epichlorohydrin carbonate) reached only up to 35% in 12 hours (entry 1, Table 1), but when the temperature was increased to 50 °C and 70 °C, the yields were

increased up to 65% (entry 2) and 96% (entry 3), respectively. Furthermore, no satisfactory results were obtained when the reaction time was increased or decreased at 70 °C (entries 4–7). Subsequently, we also investigated the influence of other factors, such as catalyst dosage (entries 8–10) and cocatalyst (entries 11 and 12), on this reaction, but no encouraging results were observed. Therefore, the reaction conditions for the cycloaddition of CO_2 to ECH were optimized as – a reaction time of 12 hours at 70 °C in the presence of a CO_2 balloon under neat conditions with a *substrate/catalyst/co-catalyst* mole ratio of 1 : 0.0115 : 0.062. Under the optimized reaction conditions, hybrids **2** and **3** yielded 94% (entry 2, Table 2) and 95% (entry 3, Table 2) of ECHC, respectively. Interestingly, when we used hybrids **1–3** as catalysts without any cocatalyst under the optimized reaction conditions, conversions of 55% (entry 9), less than 10% (entry 10), and less than 1% (entry 11), respectively, were obtained (see Table 2). Therefore, hybrid **1**, along with the cocatalyst TBAB, showed the best catalytic efficiency among all hybrids tested for the cycloaddition of CO_2 to ECH.

Several control experiments were also performed to understand the roles of the organic counterions and the decavanadate POM cluster in the observed catalysis by hybrid **1** under the optimized reaction conditions. To understand the roles of the quinolinium OCI in catalysis, we used different decavanadate cluster-based compounds with other counterions (Na and TBA) as the catalysts in place of hybrid **1**. Also, we used the quinolinium counterion precursor (ACMQI) alone as the catalyst to confirm the roles of the decavanadate cluster in the catalysis exhibited by hybrid **1**. These control experiments demonstrated that the decavanadate cluster with other counterions and ACMQI alone as catalysts yielded poor conversion of ECH (entries 6–8, Table 2) compared to the hybrid **1**-catalyzed reaction. To investigate the role of the countercation present in the cocatalyst, we tested different bromides as coca-

Scheme 2 Cycloaddition of CO_2 catalyzed by hybrids **1–3**.

Table 1 Cycloaddition of CO_2 to ECH by using TBAB and hybrid **1** as a cocatalyst and catalyst, respectively[a]

Entry	Catalyst amount (mg(mol%))	Co-catalyst amount (mg(mol%))	Temp. (°C)	Time (h)	Yield[b] (%)
1	20 (0.115)	20 (0.62)	30	12	35
2	20 (0.115)	20 (0.62)	50	12	65
3	20 (0.115)	20 (0.62)	70	12	96
4	20 (0.115)	20 (0.62)	70	6	72
5	20 (0.115)	20 (0.62)	70	9	85
6	20 (0.115)	20 (0.62)	70	18	96
7	20 (0.115)	20 (0.62)	70	24	96
8	10 (0.0575)	20 (0.62)	70	12	85
9	30 (0.1725)	20 (0.62)	70	12	90
10	40 (0.23)	20 (0.62)	70	12	90
11	20 (0.115)	30 (0.93)	70	12	98
12	20 (0.115)	40 (1.24)	70	12	>99

[a] Reaction conditions: substrate (ECH) 10 mmol; hybrid **1** (catalyst); TBAB (co-catalyst); CO_2 balloon; neat condition. [b] The yield was calculated by ^1H NMR spectroscopy.

Table 2 CO_2 cycloaddition reaction with epichlorohydrin by using different catalysts[a]

Entry	Catalyst	Co-catalyst (TBAB)	Yield[b] (%)	System
1	Hybrid **1**	Present	96	Heterogeneous
2	Hybrid **2**	Present	94	Heterogeneous
3	Hybrid **3**	Present	95	Heterogeneous
4	Hybrid **4**	Present	10	Heterogeneous
5	No catalyst	Present	43	Homogeneous
6	NaV10	Present	45	Heterogeneous
7	TBAV10	Present	51	Heterogeneous
8	ACMQI	Present	65	Homogeneous
9	Hybrid **1**	Absent	55	Heterogeneous
10	Hybrid **2**	Absent	30	Heterogeneous
11	Hybrid **3**	Absent	Trace	Heterogeneous
12	Hybrid **4**	Absent	Trace	Heterogeneous
13	$H_4SiMo_{12}O_{40}$	Absent	Trace	Homogeneous
14	$H_4SiW_{12}O_{40}$	Absent	Trace	Homogeneous

[a] Reaction condition: substrate (ECH) 10 mmol; TBAB (20 mg, 0.62 mol%); catalyst (0.115 mol%); CO_2 balloon; 12 hours (h); 70 °C. [b] The yield was calculated by ^1H NMR spectroscopy.

talysts, and the results are summarized in Table S4 of the ESI.† The results showed that tetrabutylammonium bromide (TBAB) yields the highest results, while potassium bromide (KBr) yields the lowest. This difference may be attributed to the interference of K^+ ions with the basic sites of the hybrid, hindering the interaction of these basic sites with CO_2.[50]

Additionally, we compared the simulated powder X-ray diffraction (PXRD) patterns of the counterion precursor ACMQI with those of hybrid **1** before and after catalysis; see Fig. S62 in the ESI.† Our analysis showed no significant changes in the PXRD patterns before and after catalysis. Furthermore, peaks corresponding to the counterion moiety ACMQ in the PXRD pattern of the recycled catalyst rule out any cation exchange between hybrid **1** and TBAB during catalysis. Most importantly, to check the role of the '–NH₂' functionality on the OCI in determining the catalytic properties of hybrid **1**, we also synthesized another quinolinium counterion, 4,7-(dichloromethyl) quinolinium (DCMQ), bearing a '–Cl' moiety in place of the '–NH₂' functionality on ACMQ, and clubbed it with the decavanadate cluster to generate a new hybrid, $(DCMQ)_4[H_2V_{10}O_{28}]$ (hybrid **4**), as a control compound (see Fig. S12, S16 and S18–S21, in ESI† for the characterization details of hybrid **4**). Under optimized reaction conditions, we tested hybrid **4** as a catalyst in the CO_2 cycloaddition reaction. These control experiments demonstrated that the hybrid **4**, acting as a catalyst, exhibits only a negligible conversion of ECH, both with and without a cocatalyst (entries 4 and 12, Table 2).

There are a few reports on vanadium-based POM hybrids acting as catalysts for the CO_2 cycloaddition reaction.[51–54] In the present case, NH₃-TPD (see Fig. S22(b), ESI†) analysis revealed the presence of acidic sites in hybrid **1**. It is reported that the increasing amounts of reduced vanadium centers (*i.e.,* increasing V^{4+}/V^{5+} ratio) in certain vanadium-containing catalysts can enhance their surface acidity.[31–33] V^{4+} centers may enhance the Brønsted acidity of the cluster surface by polarizing small molecules.[32] Such acidic sites may also contribute to the activation of the epoxide rings during the CO_2 cycloaddition reaction.[30,55] This assumption was supported by XPS (see Fig. S19(e), ESI†) analysis of hybrid **1**, which suggested the presence of V^{4+} in the hybrid cluster. The catalytic efficiency of a catalyst towards the CO_2 cycloaddition reaction depends not only on the presence of acidic and basic sites but also on several other factors, such as surface area, structural orientation, and the various interactions present in the catalyst.[56] Therefore, all the catalytic and control experiments suggested that hybrid **1** is the best catalyst for CO_2 cycloaddition reaction among the hybrids tested in this study, and the results are comparable with those of the other reported POV-based hybrid catalysts reported in the literature.[51,52,55,57]

Plausible reaction mechanism of CO_2 cycloaddition reaction. To understand the reaction mechanism of the CO_2 cycloaddition, we studied the reaction kinetics using ECH as a substrate and hybrid **1** as a catalyst under the optimized reaction conditions. We chose three different temperatures, 30 °C, 50 °C, and 70 °C, to calculate the reaction rate constants. The

reaction rate constants were calculated by using a first-order reaction kinetics; $\ln[A]_t = \ln[A]_0 - kt$, $\ln k = \ln A - E_a/RT$, where $[A]_0$ and $[A]_t$ correspond to initial ECH concentration and concentration after time (t), k and E_a are the rate constant and activation energy of the reaction, respectively. We plotted ln $[A]_t/\ln[A]_0$ *vs.* reaction time, and the data are presented in Fig. 3(d). The activation energy (E_a) of this reaction, calculated using the Arrhenius equation, for hybrid **1** was 62 kJ mol⁻¹; see Fig. S23(b), ESI.†

Parallel to this, we calculated the thermodynamic parameters of this reaction, including the enthalpy of activation $(\Delta H^{\#})$ and entropy of activation $(\Delta S^{\#})$, using Eyring plots. The values are presented in Table 3. Further, the Gibbs free energy $(G^{\#})$ was also calculated using the fundamental thermodynamic equation $\Delta G^{\#} = \Delta H^{\#} - T\Delta S^{\#}$ at different reaction temperatures, and the calculated $\Delta G^{\#}$ values at different reaction temperatures are presented in Fig. S23(c and d), ESI.†

The $\Delta H^{\#}$ and $\Delta G^{\#}$ (Table 3) values calculated for the formation of ECHC from CO_2 and ECH suggest that the reaction is endothermic and chemically controllable.[50] The calculated negative entropy $(\Delta S^{\#})$ value suggests an associative reaction pathway,[50] using hybrid **1** and TBAB as the catalyst and the cocatalyst, respectively.

Based on experimental evidence and literature reports, a plausible reaction mechanism for the hybrid **1**-catalyzed cycloaddition of CO_2 to epoxide is proposed, as shown in Fig. S58 of the ESI.†[51,58,59] The protons of '–NH₂' group in the counterion can interact with and activate the epoxide through hydrogen bonding interactions.[60] Additionally, the V^{4+} centers present on the decavanadate cluster may lead to the formation of some acidic sites and contribute to the activation of the epoxide.[31–33] On the other hand, the basic surface oxygens of POMs, along with the basic amine functionality on counterions, can interact with CO_2, helping to activate it.[45,61] Following these activations, the 'Br⁻' of the cocatalyst TBAB nucleophilically attacks the less crowded carbon atom of the epoxide ring, and simultaneously, the activated CO_2 is attacked by the negatively charged oxygen atom of the epoxide. Finally, the ring-closing eliminates the carbonate product and 'Br⁻' ion by regenerating the catalyst. The better catalytic performance of hybrid **1** compared to hybrids **2** and **3** can also be understood, considering its high overall negative charge and basicity due to the presence of surface oxygens.

Substrate scope of CO_2 cycloaddition reaction. The higher catalytic activity of hybrid **1** towards CO_2 cycloaddition with ECH under mild reaction conditions prompted us to explore a broader substrate scope using several other epoxides. We used various substrates, including *tert*-butyl glycidyl ether, allyl glycidyl ether, butyl glycidyl ether, styrene oxide, 1,2-epoxydecane, and 2-(phenoxymethyl)oxirane, to test the generality of the catalyst; see Table 4. Among all the epoxides tested, *tert*-butyl glycidyl ether (entry 2), allyl glycidyl ether (entry 3), and 2-(phenoxymethyl)oxirane (entry 4) showed conversions of over 92–96% to their corresponding carbonates, with higher turnover number (TON) values. Further, butyl glycidyl ether (entry 5) showed only a moderate conversion of up to 70%, probably due to the
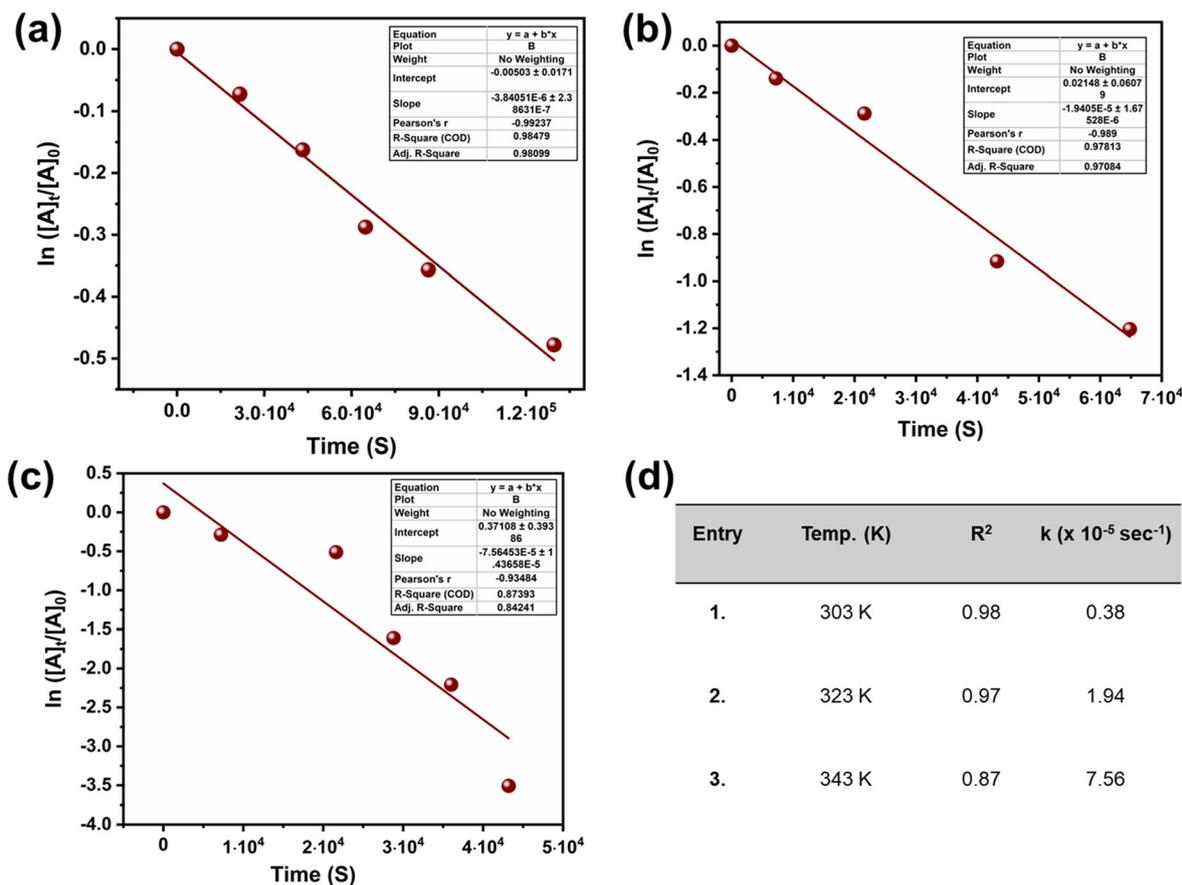
Fig. 3 Semilogarithmic plots of the ECH concentration *vs.* time at (a) 303 K; (b) 323 K; (c) 343 K; and (d) a table showing the kinetic parameters related to the CO_2 cycloaddition reaction.

Table 3 Details of thermodynamic parameters of the formation of epichlorohydrin carbonate at 70 °C

$\Delta H^{\#}$ (kJ mol^{-1})	$\Delta S^{\#}$ (J mol^{-1} K^{-1})	$\Delta G^{\#}$ (kJ mol^{-1})
61.74 ± 0.97	−144.85 ± 0.003	111.41 ± 1.095

increased chain length causing an enhancement in the non-polarity of the side chain.[62] In the case of 1,2-epoxy decane (entry 6), the conversion was even less, *i.e.*, 45%, because the bigger aliphatic chain slows down the mass transfer in the reaction system.[62] On the other hand, in the case of styrene oxide (entry 7), the product yield was lower, *i.e.*, 60%, probably due to a low reactive β-carbon atom.[63] Overall, it can be concluded that hybrid **1** can catalyze the conversion of a variety of epoxides into cyclic carbonates in good conversion yields.

Catalyst stability and recyclability. The stability and recyclability of hybrid **1** as a catalyst for the CO_2 cycloaddition reaction were analyzed using XPS, FT-IR, and PXRD analyses of the recovered catalyst after five cycles. FT-IR spectra of the recovered hybrid **1** matched with the fresh catalyst without any significant shift in the peak positions; see Fig. S40, ESI.† The XPS data revealed the presence of all the elements, including N, C,

Cl, and V, and all the deconvoluted peaks agreed with those of the fresh catalyst; see Fig. S39, ESI.† To support the structural integrity of the catalyst, we performed PXRD analysis on the recovered hybrid **1**, which also agreed with the PXRD data of the fresh catalyst; see Fig. 4(a). These experimental results collectively indicate the stability of hybrid **1** as a catalyst under the given experimental conditions.

Knoevenagel condensation reaction

The Knoevenagel condensation reaction is a crucial method for synthesizing α,β-unsaturated products using an active methylene group and carbonyl compounds.[64–66] Such α,β-unsaturated compounds are primarily utilized in the production of fine chemicals, natural products, insecticides, therapeutic agents, coumarin derivatives, polymers for the cosmetic industry, and pesticides.[18–21] In this condensation reaction, a base, such as amines or other organic or inorganic bases, abstracts a proton from an active methylene compound to generate a carbanion. At the same time, Lewis acids, such as metal chlorides, or organic moieties like primary amines, activate the carbonyl group, allowing the carbanion to attack it to form a C=C bond after dehydration of the initially formed product.[6,67–69]

Table 4 Substrate scope for the CO_2 cycloaddition reaction by using hybrid **1** as a catalyst[a]

Entry	Reactants	Products	Yield[b] (%)	Time (h)	TON[c]	TOF[d] (h^{-1})
1			96	12	834	69.5
2			92	12	800	66.6
3			94	12	817	68.08
4			95	12	826	68.83
5			70	12	608	50.66
6			45	12	391	32.58
7			60	12	521	43.41
8			61	12	530	44.20

[a] Reaction conditions: substrate (ECH) – 10 mmol; TBAB – 20 mg (0.62 mol%); catalyst – 20 mg (0.115 mol%); CO_2 balloon, at 70 °C for 12 hours. [b] The yield and the purity of the products were analyzed by ^{1}H NMR and ^{13}C NMR. [c] TON (turnover number) = moles of product/moles of catalyst. [d] TOF (turnover frequency) = TON/time (h).
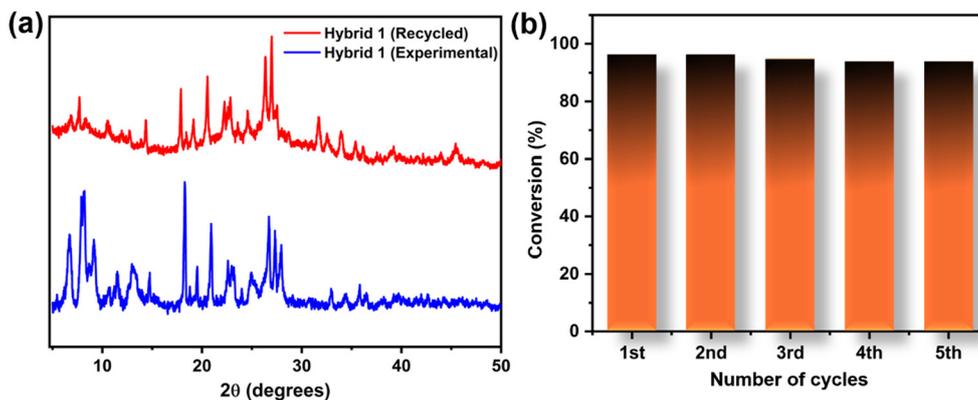
Fig. 4 (a) PXRD data of recovered catalyst after CO_2 cycloaddition; (b) catalyst recyclability (hybrid **1**) up to five cycles.

The organic counterions of the Class 1 POM hybrids can provide additional stability and help control the heterogeneity of the POM clusters in a reaction medium. Several studies have demonstrated that tuning the organic counterion functionality can significantly influence the catalytic properties of POM-hybrids.[39] To evaluate the catalytic abilities of hybrids **1–3** towards the Knoevenagel condensation reaction, we chose benzaldehyde and malononitrile as model substrates, hybrid **1** as a model catalyst, and ethanol as a solvent to obtain 2-benzylidene malononitrile at room temperature; see Scheme 3.

The catalytic reaction conditions were optimized by varying key parameters, including the solvent system, reaction temperature, catalyst dosage, and reaction time. The reaction
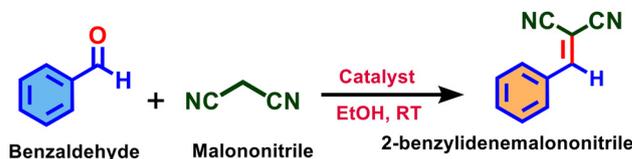
Scheme 3 Reaction scheme of Knoevenagel condensation catalyzed by hybrids **1–3**.

product yields were calculated using ^{1}H NMR spectroscopy with tetrachloroethane (TCE) as an internal standard, and the results are presented in Table 5. First, the reaction was carried

Table 5 Optimization of the conditions of Knoevenagel condensation reaction catalyzed by hybrid **1**[a]

Entry	Catalyst[a] (μmol)	Time (h)	Temp. (°C)	Conv.[b] (%)
1	2.4	2	rt	90
2	2.4	3	rt	96
3	2.4	2	35	95
4	2.4	3	35	97
5	2.4	3	45	98
6	1.2	3	rt	85
7	4.8	3	rt	96
8	2.4[c]	3	rt	30
9	2.4[d]	3	rt	85
10	2.4[e]	3	rt	92
11	2.4[f]	3	rt	60
12	2.4[g]	3	rt	<10

[a] Reaction conditions: ethanol – 1.5 mL; benzaldehyde – 0.2 mmol; malononitrile – 0.22 mmol; hybrid **1** as a catalyst – 2.4 μmol. [b] The yield was calculated by ^{1}H NMR analysis and TCE was used as an internal standard. [c] Dichloromethane (1.5 mL). [d] IPA (1.5 mL). [e] Methanol (1.5 mL). [f] Water (1.5 mL). [g] Acetonitrile as a solvent.

Table 6 Knoevenagel condensation reaction in the presence of different types of catalysts[a]

Entry	Catalyst	Conv. (%)[b]	System
1	$[H_2V_{10}O_{28}(C_{10}H_{10}ClN_2)_4]$ (Hybrid **1**)	96	Heterogenous
2	$[SiMo_{12}O_{40}(C_{10}H_{10}ClN_2)_4]$ (Hybrid **2**)	65	Heterogenous
3	$[SiW_{12}O_{40}(C_{10}H_{10}ClN_2)_4]$ (Hybrid **3**)	80	Heterogenous
4	$[H_2V_{10}O_{28}(C_{10}H_8Cl_2N)_4]$ (Hybrid **4**)	>10	Heterogenous
5	$[C_{10}H_{10}ClN_2I]$ (ACMQI)	35	Homogenous

[a] Reaction conditions: ethanol – 1.5 mL; benzaldehyde – 0.2 mmol; malononitrile – 0.22 mmol; catalyst – 2.4 μmol; at 25 °C for 3 hours. [b] The yield was calculated by ^{1}H NMR analysis and TCE was used as an internal standard.

out at different temperatures, *i.e.*, room temperature, 35 °C, and 45 °C, for 3 hours using ethanol as a solvent. In all cases, the substrate amount, catalyst dosage, and solvent volume were maintained at 0.2 mmol, 2.4 μmol, and 1.5 mL, respectively. The results indicated that at room temperature, conversion reached up to 90% in 2 hours (entry 1, Table 5) and 96% after 3 hours (entry 2). Furthermore, when the temperature was increased to 35 °C and 45 °C, a faster conversion rate was observed, yielding 97% (entry 4) and 98% (entry 5) of the products, respectively.

We also investigated other influencing reaction parameters, such as catalyst amount (entries 6 and 7) and solvent system (entries 8–12), on this reaction, but no encouraging results were obtained. Therefore, the reaction conditions for the Knoevenagel condensation reactions were optimized as follows: benzaldehyde (0.2 mmol), malononitrile (0.22 mmol), and 2.4 μmol of the catalyst in ethanol at room temperature (25 °C) for 3 hours. Subsequently, we tested the catalytic ability of hybrids **2** and **3** towards Knoevenagel condensation under the optimized reaction conditions. They yielded 65% (entry 2, Table 6) and 80% (entry 3, Table 6). Therefore, the catalytic activity order of the hybrids towards the Knoevenagel condensation reaction was hybrid **1** > hybrid **3** > hybrid **2**.

Hence, hybrid **1** exhibited the best catalytic activity toward the Knoevenagel condensation reaction among all the tested hybrids and was comparable to, or better than, other POV-based hybrid catalysts reported in the literature.[8,70] To better understand the role of the amine functional group on the OCIs, we tested hybrid **4** as a catalyst under the optimized reaction conditions. Furthermore, to understand the role of the decavanadate cluster in the observed catalysis by hybrid **1**, we also tested the counterion precursor, ACMQI, as a catalyst under the optimized reaction conditions (see Table 6). The results indicated that the hybrid **4**, as a catalyst, yielded only a trace amount of product (~10%) (entry 4), while ACMQI yielded 35% (entry 5). Therefore, we can conclude that the

amine functionality on the OCI of hybrid **1** boosted the system's basicity,[71] which further affected the Knoevenagel condensation reaction. Similarly, the decavanadate cluster also plays a significant role in activating the substrates in this reaction.

Kinetics of Knoevenagel condensation reaction. To evaluate the reaction kinetics using hybrid **1** as a catalyst, we chose three reaction temperatures, 25 °C, 35 °C, and 45 °C (see Fig. 5). The reaction rate constants at these temperatures were calculated using the pseudo-first-order reaction kinetics: $\ln(C_0/C_t) = kt$ and $\ln k = -E_a/RT$, where C_0 and C_t correspond to the initial concentration of benzaldehyde and concentration at a different reaction time (t), respectively; k and E_a represents the rate constant and the activation energy, respectively. The plot of $\ln(C_0/C_t)$ *vs.* reaction time (t) showed linearity; see Fig. S37(a) in the ESI.† All kinetics-related data are presented in Fig. S38 of the ESI.† The activation energy (E_a) for the reaction using hybrid **1** as a catalyst was calculated using the Arrhenius equation. Hybrid **1** showed an activation energy of 34.12 kJ mol^{-1} in the Knoevenagel condensation reaction; see Fig. S37(b), ESI.†

Plausible mechanism of Knoevenagel condensation reaction. Based on the above observations and literature reports, a plausible mechanism for Knoevenagel condensation catalyzed by hybrid **1** is proposed, which follows a two-component mechanistic pathway as previously reported.[8,70,72] The carbonyl group (C=O) of benzaldehyde interacts with the amine proton of the counterions *via* a hydrogen bonding interaction, enhancing the electrophilicity of the carbonyl carbon.[6] The acidic sites on the cluster due to V^{4+} centers may also contribute to activating the carbonyl carbon. At the same time, the basic sites such as the cluster oxygens of the POM cluster or the amine functional group on the counterion[28] abstract a proton from the methylene group of malononitrile, generating a carbanion. The attack of the carbonyl group by the carbanion, followed by the liberation of one water unit, results in the formation of 2-benzylidene malononitrile as the product, along with the catalyst regeneration; see Fig. S59, ESI.†
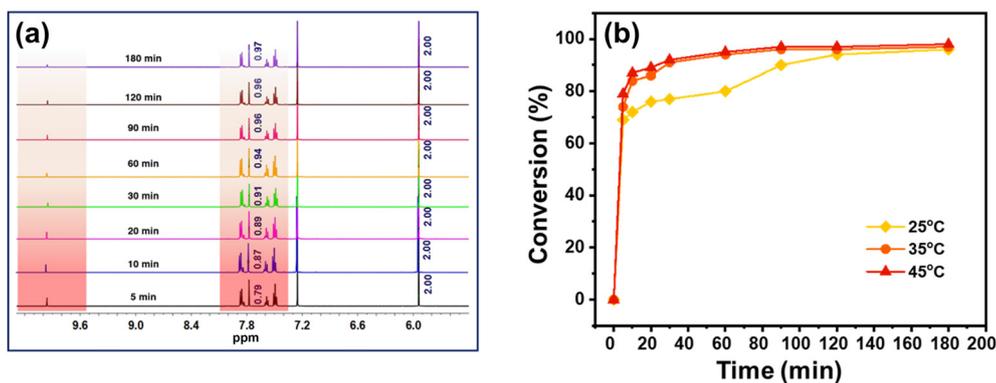
Fig. 5 (a) ^{1}H NMR spectra of benzaldehyde conversion at different time intervals at 25 °C; (b) effect of reaction temperature on the catalytic performance of hybrid **1**.

Substrate scope of Knoevenagel condensation reaction. Different types of aromatic aldehydes were chosen as substrates to check the substrate scope and explore the electronic and Steric effects of the substrates on the catalytic efficiency of hybrid **1** in the Knoevenagel condensation reaction. The yields of the corresponding products varied from 85% to 99%, as shown in Table 7. Particularly, the aldehydes with electron-donating substituents such as '–OMe' (entries 8 and 11), '–Me' (entry 9), and '–SMe' (entry 10) showed good conversion. Besides that, the effects of *ortho* and *meta* substituents on the aromatic aldehydes have also been studied, and it was found that the *para*-, *ortho*, and *meta*-substituted aldehydes give comparable yields.[6] Overall, it can be concluded that hybrid **1**, as a catalyst, can convert a variety of aldehydes into α- and β-unsaturated products with comparable conversion yields.

Catalyst stability and recyclability. To assess the stability and recyclability of hybrids **1–3** as catalysts for the Knoevenagel condensation reaction, hybrid **1** was selected as a model catalyst. We performed XPS and PXRD analyses on the recovered catalyst after five catalytic cycles to assess its recyclability. The XPS data revealed that all the elements, including N, C, Cl, and V, were present, and all the deconvoluted peaks agreed with those of the as-synthesized catalyst; see Fig. S54, ESI.† The FT-IR data showed stretching frequencies of the counter-ion and decavanadate cluster at the frequencies observed in the as-synthesized catalyst without having significant shifts; see Fig. S53, ESI.† The PXRD data of the recovered catalyst showed peaks similar to those of the as-synthesized catalyst at lower 2θ values. However, the recovered catalyst showed broad peaks after 12° (2θ), indicating reduced crystallinity after catalysis. At the same time, the chemical integrity of the recovered catalyst was supported by XPS and FT-IR analysis; see Fig. 6(a).

Experimental section

Materials and methods

Phenol and ammonium bicarbonate were purchased from SRL Chemicals. 4,7-Dichloro quinoline, sodium metavanadate

(NaVO$_3$·2H$_2$O), silicotungstic acid, iodomethane, and tetrabutylammonium bromide were purchased from CDH India. Silicomolybdic acid (99%), epichlorohydrin (99%), allyl glycidyl ether (99%), butyl glycidyl ether (99%) and 1,2-epoxy-3-phenyl propane (99%) were purchased from Sigma-Aldrich, while styrene oxide (97%), tertbutyl glycidyl ether (98%) and 1,2-epoxy-dodecane (97%) were purchased from TCI chemicals. 4,7-Dichloroquinoline was procured from CDH Chemicals. All the NMR solvents, such as CDCl$_3$ (99.80% D), DMSO-d_6 (99.80% D), were purchased from Sigma Aldrich, and hexane was used after distillation. All other chemicals were used as received without further purification.
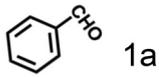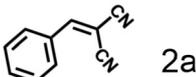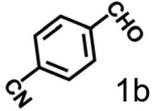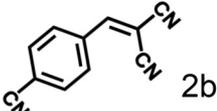
Physical measurements

^{1}H, ^{13}C, and ^{29}Si NMR spectra were recorded on a JEOL-JNM-500 MHz NMR spectrometer using CDCl$_3$ and DMSO-d$_6$ solvents, with TMS as the internal standard. FT-IR spectra were recorded on the Agilent Technology Cary 600 series instrument. ESI-MS spectra were recorded on a Bruker HD compact instrument. Thermogravimetric analyses (TGA) were performed using the PerkinElmer Pyris 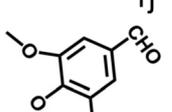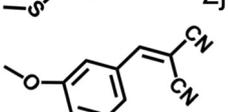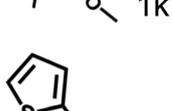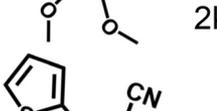1 instrument. The samples (1.5 mg) were heated under a nitrogen atmosphere from room temperature to 800 °C at a heating rate of 10 °C min^{-1} with a flow rate of 20 mL min^{-1} in all the TGA experiments. Nitrogen and carbon dioxide physisorption isotherms were evaluated using the Autosorb-iQ-MP/XR model of the Quantachrome instrument. X-ray photoelectron spectroscopy (XPS) was conducted on a ThermoFisher Scientific NEXSA photoelectron spectrometer equipped with the Al Kα (1486.6 eV) dual anode as the source. The spectrometer operated at a 12 kV anode voltage and 6.50 mA filament current. The XPS data were collected with a pass energy of 50 eV under a vacuum of 9×10^{-8} bar, using Avantage software for analysis.

X-ray crystallography

Single crystal X-ray diffraction data of hybrids **1–3** were collected on an Agilent SuperNova diffractometer equipped with multilayer optics, monochromatic dual source (Cu and Mo), and Eos CCD detector, using Mo Kα (0.71073 Å) radiation at

Table 7 Substrate scope for Knoevenagel condensation reaction catalyzed by hybrid **1**[a]

Entry	Carbonyl compound	Product	Time (h)	Yield[b] (%)	TON[c]	TOF[d] (h^{-1})
1	**1a**	**2a**	3	96%	5647.05	1882.36
2	**1b**	**2b**	3	99%	5823.52	1941.17
3	**1c**	**2c**	3	97%	5705.88	1901.96
4	**1d**	**2d**	3	95%	5588.23	1862.74
5	**1e**	**2e**	3	98%	5764.70	1921.56
6	**1f**	**2f**	3	98%	5764.70	1921.56
7	**1g**	**2g**	3	98%	5764.70	1921.56
8	**1h**	**2h**	3	90%	5294.11	1764.7
9	**1i**	**2i**	3	98%	5764.70	1921.56
10	**1j**	**2j**	3	99%	5823.52	1941.17
11	**1k**	**2k**	3	85%	5000	1666.66
12	**1l**	**2l**	3	91%	5352.94	1784.31
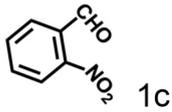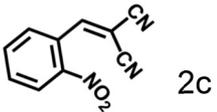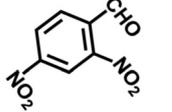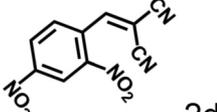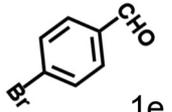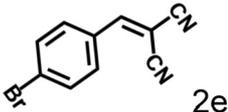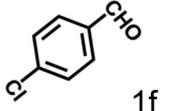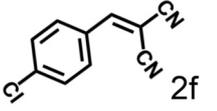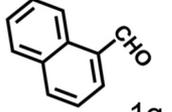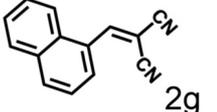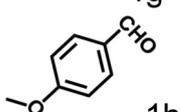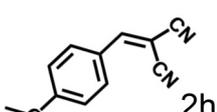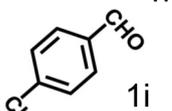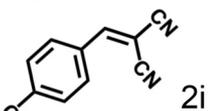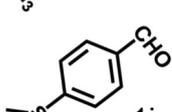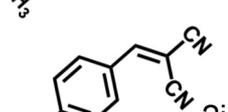
[a] Reaction conditions: ethanol – 1.5 mL; aldehyde – 0.2 mmol; malononitrile – 0.22 mmol; catalyst (hybrid **1**) – 2.4 μmol; at 25 °C for 3 h. [b] The yield and the purity of the products were analyzed by ¹H NMR using TCE as an internal standard. [c] TON (turnover number) = mole of product/mole of catalyst. [d] TOF (turnover frequency) = TON/time (h).
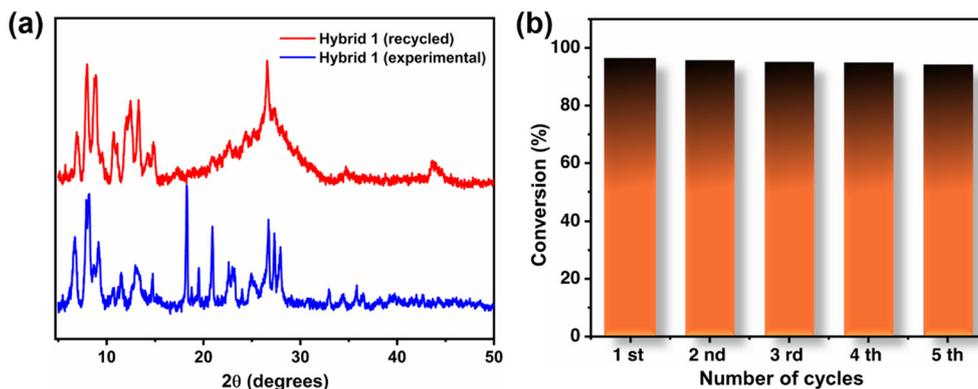
Fig. 6 (a) PXRD data of recovered catalyst; (b) recyclability of catalyst (hybrid **1**) up to five cycles.

293 K. Data acquisition, reduction, and analytical face-index-based absorption correction were performed by using the CrysAlisPRO program.[73] The structures were solved with ShelXS and refined on F^2 using full-matrix least-squares techniques with the ShelXL program, provided in the Olex^2 (v.1.2) program package.[74,75] Anisotropic displacement parameters were applied for all the atoms, except hydrogen atoms and some less intensely scattered carbon atoms. CCDC no: 2390257, 2390258 and 2390259† contain supplementary crystallographic data of hybrids **1**, **2** and **3**, respectively.

Synthesis and characterisation of organic counter ions (OCIs)

Synthesis of 4-amino 7-chloroquinoline. 4-Amino 7-chloroquinoline was synthesized by following a reported procedure.[76] Yield: 670 mg, 75%. ^{1}H NMR (500 MHz, CDCl$_3$): δ ppm 8.53 (d, 1H, $J = 5$ Hz, ArH), 7.9 (d, 1H, $J = 5$ Hz, ArH), 7.69 (d, 1H, $J = 5$ Hz, ArH), 7.4 (m, 1H, ArH), 6.58 (d, 1H, $J = 5$ Hz, ArH). ^{13}C NMR (125 MHz, CDCl$_3$): 151.75, 149.53, 149.46, 135.25, 128.79, 125.69, 121.63, 117.08, 103.96. ESI-MS: calcd for C$_9$H$_7$ClN$_2^+$ [M + H]$^+$, 179.03; found, 179.0630.

Synthesis of 4-amino-7-chloro-1-methylquinolin-1-ium iodide (ACMQI). ACMQI was synthesized by dissolving 4-amino 7-chloroquinoline in methanol and refluxing it overnight with iodomethane. The product was precipitated as a white solid, which was collected, washed several times with methanol and diethyl ether followed by drying at 50 °C. Yield: 1.5 g, 94%. ^{1}H NMR (500 MHz, DMSO-D$_6$): δ ppm 9.07 (d, 2H, $J = 10$ Hz, Ar–NH$_2$), 8.48 (t, 2H, $J = 10$ Hz, ArH), 8.19 (d, 1H, ArH), 7.86 (m, 1H, ArH), 6.77 (d, 1H, $J = 10$ Hz, ArH), 4.08 (s, 3H, –CH$_3$). ^{13}C NMR (125 MHz, DMSO-D$_6$): 157.68, 147.36, 139.85, 139.39, 126.93, 126.37, 118.18, 115.60, 102.37, 42.13. ESI-MS: calcd for C$_{10}$H$_{10}$ClN$_2^+$ [M]$^+$, 193.05; found, 193.0732. FT-IR (cm^{-1}) (s = strong, m = medium, w = weak, br = broad): 3449 (br), 3274 (s), 3124 (s), 3034 (s), 1647 (s), 1617 (s), 1536 (m), 1471 (m), 1229 (s). 1039 (m), 872 (m) – 579 (m).

Synthesis of 4,7-dichloro-1-methylquinolin-1-ium iodide (DCMQI). DCMQI was synthesized following a reported procedure.[77] Yield: 1.2 g, 71%. ^{1}H NMR (500 MHz, DMSO-D$_6$): δ ppm 8.92 (d, 1H, $J = 5$ Hz, ArH), 8.72 (d, 1H, $J = 5$ Hz, ArH), 8.54 (d, 1H, $J = 5$ Hz, ArH), 8.34 (d, 1H, $J = 10$ Hz, ArH), 8.07 (m,

1H, ArH), 4.43 (s, 3H, –CH$_3$). ^{13}C NMR (125 MHz, DMSO-D$_6$): 149.11, 141.99, 138.08, 136.28, 134.01, 132.64, 131.03, 128.62, 119.86, 46.11. ESI-MS: calcd for C$_{10}$H$_8$Cl$_2$N$^+$ [M]$^+$, 212.00; found, 212.0195. FT-IR (cm^{-1}) (s = strong, m = medium, w = weak, br = broad): 3061 (m), 2979 (w), 2922 (m), 1597 (s), 1559 (s), 1412 (m), 1350 (s), 1184 (m), 1084 (s). 833 (s).

General procedure for the synthesis of hybrids 1 and 4

NaVO$_3$·2H$_2$O (0.5 g, 4.10 mmol) was dissolved in 20 mL of DI water and heated to 70 °C for a clear, colourless solution. The solution was cooled down to room temperature. 4 M HCl was added to the solution, and the pH was maintained at 4.5. At this point, the color of the solution changed to orange, indicating the formation of decavanadate. Parallel to this, the ACMQI (68 mg, 0.213 mmol) counterion was dispersed in a 5 mL mixture of ethanol and water (1 : 1). This dispersion was added dropwise to the decavanadate solution, leading to the formation of an instant yellow precipitate, which was stirred overnight at room temperature. After this, the reaction mixture was filtered, and the resulting precipitate was washed thoroughly with water, ethanol, and diethyl ether, and then dried at 50 °C under vacuum to obtain hybrid **1**. For crystallization, hybrid **1** was dissolved in DMF and allowed to slowly evaporate. After a few weeks, bright orange crystals were obtained from the mother liquor. These crystals were washed several times with ethanol and diethyl ether and then dried under vacuum for characterization.

Hybrid **4** was also synthesized using a similar procedure to that used for hybrid **1**, starting from [H$_2$V$_{10}$O$_{28}$]$^{4-}$ and using the counterion precursor DCMQI in place of ACMQI.

(ACMQ)$_4$[H$_2$V$_{10}$O$_{28}$] (hybrid 1). Yield: 15% based on V. ^{1}H NMR (500 MHz, DMSO-d$_6$): ACMQ$^+$ cations: δ ppm 9.09 (b, 2H, Ar–NH$_2$), 8.50 (m, 2H, Ar–H), 8.13 (s, 1H, Ar–H), 7.83 (d, 1H, $J = 5$ Hz, Ar–H), 6.82 (d, 1H, $J = 5$ Hz, Ar–H), 4.06 (s, 3H, –CH$_3$). FT-IR (cm^{-1}): 3330 (br), 3161 (br), 3081 (s), 1658 (w), 1616 (s), 1510 (m), 1462 (s), 1368 (m), 1209 (s), ν (V=O, V–O–V), 948 (s), 819 (s), 731 (w), 542 (m), 512 (w), 454 (m).

(DCMQ)$_4$[H$_2$V$_{10}$O$_{28}$] (hybrid 4). Yield: 28% based on V. ^{1}H NMR (500 MHz, DMSO-d$_6$): δ ppm DCMQ$^+$ cations: 9.10 (d, 1H, $J = 5$ Hz, ArH), 8.84 (d, 1H, $J = 5$ Hz, ArH), 8.63 (d, 1H, Ar–

H), 8.35 (d, 1H, J = 10 Hz, ArH), 8.09 (m, 1H, Ar–H), 4.51 (s, 3H, –CH$_3$). FT-IR (cm^{-1}): 3048 (m), 2943 (w), 1589 (s), 1552 (s), 1505 (s), 1353 (s), 1090 (s), ν (V=O, V–O–V), 954 (s), 810 (s), 738 (s), 590 (m), 457 (w).

General procedure for the synthesis of hybrids 2 and 3

Commercially available POM, silicomolybdic acid [H$_4$SiMo$_{12}$O$_{40}$] (100 mg, 0.054 mmol), was dissolved in 20 mL DI water. The counterion precursor ACMQI (78 mg, 0.243 mmol) was dispersed in a 5 mL mixture of ethanol and water (1 : 1; v/v). This dispersion was then slowly added to the POM solutions, stirred continuously in the dark overnight, to obtain a light-yellow precipitate of hybrid **2**. The precipitate was filtered and washed several times with water, ethanol, and ether, and dried under vacuum at 50 °C.

Hybrid **3** was also synthesized using a similar procedure to that used for hybrid **2**, starting from the POM cluster [H$_4$SiW$_{12}$O$_{40}$] (100 mg, 0.034 mmol) in place of the POM cluster [H$_4$SiMo$_{12}$O$_{40}$] and with ACMQI (49 mg, 0.153 mmol).

(ACMQ)$_4$[SiMo$_{12}$O$_{40}$] (hybrid 2). Yield: 58% based on Mo. ^{1}H NMR (500 MHz, DMSO-d$_6$): ACMQ$^+$ cations: δ ppm 9.05 (d, 2H, J = 20 Hz, Ar–NH$_2$), 8.45 (m, 2H, Ar–H), 8.15 (s, 1H, Ar–H), 7.83 (m, 1H, Ar–H), 6.74 (d, 1H, J = 10 Hz, Ar–H), 4.06 (s, 3H, –CH$_3$), ^{29}Si NMR (100 MHz, DMSO-d$_6$) δ ppm −110.90. FT-IR (cm^{-1}): 3340 (br), 3233 (m), 3128 (br), 1646 (s), 1599 (s), 1533 (m), 1463 (br), 1351 (m), 1233 (s), ν (M=O, Mo–O–Mo), 943(m), 890 (s), 785 (s), 601 (m), 508 (w), 452 (w).

(ACMQ)$_4$[SiW$_{12}$O$_{40}$] (hybrid 3). Yield: 78% based on W. ^{1}H NMR (500 MHz, DMSO-d$_6$): δ ppm ACMQ$^+$ cations: 9.05 (b, 2H, Ar–NH$_2$), 8.45 (b, 1H, Ar–H), 8.16 (s, 1H, Ar–H), 7.83 (b, 1H, Ar–H), 6.74 (m, 1H, Ar–H), 4.05 (s, 3H, –CH$_3$), ^{29}Si NMR (100 MHz, DMSO-d$_6$) δ ppm −110.88. FT-IR (cm^{-1}): 3464 (br), 3358 (br), 3210 (br), 3087 (br), 1647 (s), 1616 (s), 1535 (m), 1451 (br), 1363 (m), 1239 (s), ν (W=O, W–O–W), 967(m), 914 (s), 873 (w), 778 (s), 530 (m).

Conclusions

In this work, we have developed a new organic counterion belonging to the rarely explored class of quinolinium compounds, which bears a task-specific '–NH$_2$' functional group. A series of POM clusters, including the commercially available Mo and W-based Keggin clusters [SiMo$_{12}$O$_{40}$]$^{4-}$ and [SiW$_{12}$O$_{40}$]$^{4-}$, and vanadium-based decavanadate cluster [H$_2$V$_{10}$O$_{28}$]$^{4-}$, were clubbed with the quinolinium counterion to prepare a series of POM hybrids. The bifunctional catalytic properties of the newly developed hybrids were tested toward two organic transformation reactions of contemporary relevance, the CO$_2$ cycloaddition reaction and the Knoevenagel condensation reaction. In CO$_2$ cycloaddition to ECH, the quinolinium-decavanadate hybrid exhibited the best catalytic activity, yielding 96% product conversion under ambient temperature and atmospheric pressure. The Lewis basic nature and proton donation ability of the '–NH$_2$' moiety on the quinolinium counterion are expected to play significant roles in the

observed catalytic properties of this hybrid. Hybrid **1** also exhibited good catalytic activity in the Knoevenagel condensation of benzaldehyde and malononitrile, using ethanol as the solvent at room temperature. Although hybrid **1**, with an amine functionality on the quinolinium counterion, exhibited excellent catalytic activity in both the organic transformation reactions tested, an analogous decavanadate-based control compound, hybrid **4**, with a halogen (–Cl) functionality on quinolinium counterion in place of the amine (–NH$_2$) functionality showed low activity towards both these reactions. This observation highlighted the importance of the amine functionality on the counterion in the catalytic reactions. Our strategy of incorporating task-specific functional groups on the counterion moiety of POM-based organic–inorganic hybrids opens up new possibilities for catalytic reactions in broader aspects. Furthermore, the quinolinium POM hybrids are a less-explored class of compounds in POM chemistry. Hence, there is considerable potential for developing this class of compounds with different quinolinium derivatives and POM units for diverse materials and catalytic applications in the future.

Conflicts of interest

The authors declare that they have no conflict of interest.

Data availability

The data supporting this article have been included as part of the ESI.†

Acknowledgements

References

1 A. Corma, S. B. A. Hamid, S. Iborra and A. Velty, *J. Catal.*, 2005, **234**, 340–347.
2 K. Cai, W. Tan, N. Zhao and H. He, *Cryst. Growth Des.*, 2020, **20**, 4845–4851.
3 J. Li, C. Wei, Y. Han, Y. Mei, X. Cheng, X. Huang and C. Hu, *Dalton Trans.*, 2021, **50**, 10082–10091.
4 S. Bi, F. Meng, D. Wu and F. Zhang, *J. Am. Chem. Soc.*, 2022, **144**, 3653–3659.
5 A. Wojtaszek-Gurdak, V. Calvino-Casilda, A. Grzesinska, R. Martin-Aranda and M. Ziolek, *Microporous Mesoporous Mater.*, 2019, **280**, 288–296.
6 K. Kumari, P. Choudhary, D. Sharma and V. Krishnan, *Ind. Eng. Chem. Res.*, 2023, **62**, 158–168.

7 E. Priede, S. Brica, E. Bakis, N. Udris and A. Zicmanis, *New J. Chem.*, 2015, **39**, 9132–9142.

8 H. An, J. Zhang, S. Chang, Y. Hou and Q. Zhu, *Inorg. Chem.*, 2020, **59**, 10578–10590.

9 S. Liu, H. Chen, L. Fan and X. Zhang, *Inorg. Chem.*, 2023, **62**, 3562–3572.

10 Z.-Z. Yang, L.-N. He, J. Gao, A.-H. Liu and B. Yu, *Energy Environ. Sci.*, 2012, **5**, 6602–6639.

11 H. Chand, P. Choudhary, A. Kumar, A. Kumar and V. Krishnan, *J. CO₂ Util.*, 2021, **51**, 101646.

12 Y. Lei, H. Q. N. Gunaratne and L. Jin, *J. CO₂ Util.*, 2022, **58**, 101930.

13 X. Liao, F.-C. Cui, J.-H. He, W.-M. Ren, X.-B. Lu and Y.-T. Zhang, *Chem. Sci.*, 2022, **13**, 6283–6290.

14 Y. Qian, Y. Chu, Z. Zheng, Z. Shadike, B. Han, S. Xiang, Y. Kang, S. Hu, C. Cao, L. Zhong, Q. Shi, M. Lin, H. Zeng, J. Wang, E. Hu, C. Weiland, X.-Q. Yang and Y. Deng, *Energy Storage Mater.*, 2022, **45**, 14–23.

15 D. C. Webster and A. L. Crain, *Prog. Org. Coat.*, 2000, **40**, 275–282.

16 S. Samanta and R. Srivastava, *Mater. Adv.*, 2020, **1**, 1506–1545.

17 F. Freeman, *Chem. Rev.*, 1980, **80**, 329–350.

18 M. Zahouily, M. Salah, B. Bahlaouane, A. Rayadh, A. Houmam, E. A. Hamed and S. D. Sebti, *Tetrahedron*, 2004, **60**, 1631–1635.

19 L. F. Tietze and N. Rackelmann, *Pure Appl. Chem.*, 2004, **76**, 1967–1983.

20 G. A. Kraus and M. E. Krolski, *J. Org. Chem.*, 1986, **51**, 3347–3350.

21 F. Liang, Y.-J. Pu, T. Kurata, J. Kido and H. Nishide, *Polymer*, 2005, **46**, 3767–3775.

22 S. Himeno, M. Takamoto, R. Santo and A. Ichimura, *Bull. Chem. Soc. Jpn.*, 2005, **78**, 95–100.

23 K. Liu, Z. Yao, H. N. Miras and Y.-F. Song, *ChemCatChem*, 2015, **7**, 3903–3910.

24 K. Suzuki, M. Sugawa, Y. Kikukawa, K. Kamata, K. Yamaguchi and N. Mizuno, *Inorg. Chem.*, 2012, **51**, 6953–6961.

25 W. Ge, X. Wang, L. Zhang, L. Du, Y. Zhou and J. Wang, *Catal. Sci. Technol.*, 2016, **6**, 460–467.

26 S. Hayashi, S. Yamazoe, K. Koyasu and T. Tsukuda, *RSC Adv.*, 2016, **6**, 16239–16242.

27 S. Hayashi, S. Yamazoe, K. Koyasu and T. Tsukuda, *Chem. – Asian J.*, 2017, **12**, 1635–1640.

28 K. Sugahara, T. Kimura, K. Kamata, K. Yamaguchi and N. Mizuno, *Chem. Commun.*, 2012, **48**, 8422–8424.

29 J. Lu, X. Ma, V. Singh, Y. Zhang, P. Wang, J. Feng, P. Ma, J. Niu and J. Wang, *Inorg. Chem.*, 2018, **57**, 14632–14643.

30 J.-P. Cao, Y.-S. Xue, N.-F. Li, J.-J. Gong, R.-K. Kang and Y. Xu, *J. Am. Chem. Soc.*, 2019, **141**, 19487–19497.

31 T. Boningari, R. Koirala and P. G. Smirniotis, *Appl. Catal. Environ.*, 2013, **140–141**, 289–298.

32 G.-J. Dong, Y. Bai, Y.-F. Zhang and Y. Zhao, *New J. Chem.*, 2015, **39**, 3588–3596.

33 X. Zhao, Y. Yan, L. Mao, M. Fu, H. Zhao, L. Sun, Y. Xiao and G. Dong, *RSC Adv.*, 2018, **8**, 31081–31093.

34 A. Dolbecq, E. Dumas, C. R. Mayer and P. Mialane, *Chem. Rev.*, 2010, **110**, 6009–6048.

35 K. Routh, S. Kaur and C. P. Pradeep, *Eur. J. Inorg. Chem.*, 2022, **2022**, e202200265.

36 A. Kar and C. P. Pradeep, *Dalton Trans.*, 2020, **49**, 12174–12179.

37 L. Huder, C. Rinfray, D. Rouchon, A. Benayad, M. Baraket, G. Izzet, F. Lipp-Bregolin, G. Lapertot, L. Dubois, A. Proust, L. Jansen and F. Duclairoir, *Langmuir*, 2016, **32**, 4774–4783.

38 Q. Peng, J. Chen, T. Wang, L. Gong, X. Peng, M. Wu, Y. Ma, F. Wu, D. Yang, H. Zhang and H. Zeng, *J. Mater. Chem. A*, 2021, **9**, 12988–13000.

39 K. Routh and C. P. Pradeep, *Inorg. Chem.*, 2023, **62**, 13775–13792.

40 X.-M. Chen, Y.-L. Huang, Q. Cai, Y.-Z. Han and Q. Deng, *J. Cluster Sci.*, 2015, **26**, 1943–1957.

41 J. Cuan and B. Yan, *RSC Adv.*, 2013, **3**, 20077–20084.

42 Z. Mao, M. Rashwan, E. Garrido Ribó, M. Nord, L. N. Zakharov, T. W. Surta, A. Uysal and M. Nyman, *J. Am. Chem. Soc.*, 2024, **146**, 19489–19498.

43 W. Ge, X. Wang, L. Zhang, L. Du, Y. Zhou and J. Wang, *Catal. Sci. Technol.*, 2016, **6**, 460–467.

44 R. Abazari, S. Sanati, A. Morsali, A. M. Kirillov, A. M. Z. Slawin and C. L. Carpenter-Warren, *Inorg. Chem.*, 2021, **60**, 2056–2067.

45 H. M. Lee, I. S. Youn, M. Saleh, J. W. Lee and K. S. Kim, *Phys. Chem. Chem. Phys.*, 2015, **17**, 10925–10933.

46 H. Tong, Y. Qu, Z. Li, J. He, X. Zou, Y. Zhou, T. Duan, B. Liu, J. Sun and K. Guo, *Chem. Eng. J.*, 2022, **444**, 135478.

47 B. Zou and C. Hu, *Curr. Opin. Green Sustainable Chem.*, 2017, **3**, 11–16.

48 Y.-M. Shen, W.-L. Duan and M. Shi, *Eur. J. Org. Chem.*, 2004, 3080–3089.

49 X. Wu, C. Chen, Z. Guo, M. North and A. C. Whitwood, *ACS Catal.*, 2019, **9**, 1895–1906.

50 A. Eskemech, H. Chand, A. Karmakar, V. Krishnan and R. R. Koner, *Inorg. Chem.*, 2024, **63**, 3757–3768.

51 X. Huang, X. Gu, H. Zhang, G. Shen, S. Gong, B. Yang, Y. Wang and Y. Chen, *J. CO₂ Util.*, 2021, **45**, 101419.

52 B.-B. Lu, J. Yang, Y.-Y. Liu and J.-F. Ma, *Inorg. Chem.*, 2017, **56**, 11710–11720.

53 J. Wang, H. Xu, Q. Wang, J. Zhou, X. Xiang, S. Li, H. Mei and Y. Xu, *Chem. Eng. J.*, 2023, **474**, 145662.

54 C.-C. Zhao, X.-F. Su, R.-H. Li, L.-K. Yan and Z.-M. Su, *Inorg. Chem.*, 2024, **63**, 14032–14039.

55 J. Wang, J. Cao, Z. Du, X. Liu, J. Li, Q. Ping, T. Zang and Y. Xu, *Chin. Chem. Lett.*, 2023, **34**, 106917.

56 S. Chowdhury, A. Sharma, P. P. Das, P. Rathi and P. F. Siril, *J. Colloid Interface Sci.*, 2024, **665**, 988–998.

57 Y.-H. Zhu, J.-B. Yang, X.-M. Liu, J.-L. Wang, Q.-D. Ping, Z.-Y. Du, J.-N. Li, T.-T. Zang, H. Mei and Y. Xu, *Dalton Trans.*, 2022, **51**, 3502–3511.

58 A. Coletti, C. J. Whiteoak, V. Conte and A. W. Kleij, *ChemCatChem*, 2012, **4**, 1190–1196.

59 X. Jiang, W. Jianyong, M. Fu, F. Wu, H. Zhang and Q. He, *Sci. Adv. Mater.*, 2019, **11**, 1140–1145.

60 H. Chand, A. Kumar, S. Goswami and V. Krishnan, *Fuel*, 2024, **357**, 129757.

61 K. Kamata and K. Sugahara, *Catalysts*, 2017, **7**(11), 345.

62 T. Biswas, A. Halder, K. S. Paliwal, A. Mitra, G. Tudu, R. Banerjee and V. Mahalingam, *Chem. – Asian J.*, 2020, **15**, 1683–1687.

63 J. Sun, S.-I. Fujita, F. Zhao and M. Arai, *Green Chem.*, 2004, **6**, 613–616.

64 D. Elhamifar, S. Kazempoor and B. Karimi, *Catal. Sci. Technol.*, 2016, **6**, 4318–4326.

65 G. Li, J. Xiao and W. Zhang, *Green Chem.*, 2012, **14**, 2234–2242.

66 A. Wach, M. Drozdek, B. Dudek, E. Szneler and P. Kuśtrowski, *Catal. Commun.*, 2015, **64**, 52–57.

67 J. N. Appaturi, R. Ratti, B. L. Phoon, S. M. Batagarawa, I. U. Din, M. Selvaraj and R. J. Ramalingam, *Dalton Trans.*, 2021, **50**, 4445–4469.

68 P. Dehghani, D. Elhamifar and S. Kargar, *Sci. Rep.*, 2025, **15**, 2873.

69 S. Johari, M. R. Johan and N. G. Khaligh, *Org. Biomol. Chem.*, 2022, **20**, 2164–2186.

70 C. Li, D. Zhong, X. Huang, G. Shen, Q. Li, J. Du, Q. Li, S. Wang, J. Li and J. Dou, *New J. Chem.*, 2019, **43**, 5813–5819.

71 Y. Gu, Q. Li, D. Zang, Y. Huang, H. Yu and Y. Wei, *Angew. Chem., Int. Ed.*, 2021, **60**, 13310–13316.

72 M.-Y. Dou, D.-D. Zhong, X.-Q. Huang and G.-Y. Yang, *CrystEngComm*, 2020, **22**, 4147–4153.

73 A. Kumar, A. K. Gupta, M. Devi, K. E. Gonsalves and C. P. Pradeep, *Inorg. Chem.*, 2017, **56**, 10325–10336.

74 O. V. Dolomanov, L. J. Bourhis, R. J. Gildea, J. A. K. Howard and H. Puschmann, *J. Appl. Crystallogr.*, 2009, **42**, 339–341.

75 G. Sheldrick, *Acta Crystallogr., Sect. A: Found. Crystallogr.*, 2008, **64**, 112–122.

76 R. C. Elderfield, W. J. Gensler, O. Birstein, F. J. Kreysa, J. T. Maynard and J. Galbreath, *J. Am. Chem. Soc.*, 1946, **68**, 1250–1251.

77 D. Galanakis, C. A. Davis, C. R. Ganellin and P. M. Dunn, *J. Med. Chem.*, 1996, **39**, 359–370.